Supporting Information for

Tunable Vapor-Condensed Nanolenses

Euan McLeod,[a,b] Chau Nguyen,[c] Patrick Huang,[b] Wei Luo,[a,b] Muhammed Veli,[a] and Aydogan Ozcan[a,b,d,e,1]

[a] Electrical Engineering Department, University of California, Los Angeles, CA, 90095, USA

[b] Bioengineering Department, University of California, Los Angeles, CA, 90095, USA

[c] Chemistry & Biochemistry Department, University of California, Los Angeles, CA, 90095, USA

[d] California NanoSystems Institute, University of California, Los Angeles, CA, 90095, USA

[e] Department of Surgery, David Geffen School of Medicine, University of California, Los Angeles, CA, 90095, USA

[1] ozcan@ucla.edu ; http://innovate.ee.ucla.edu/

This file contains 7 supporting figures, a supporting methods section on modeling the shape of isolated nanolenses, and a supporting references section.

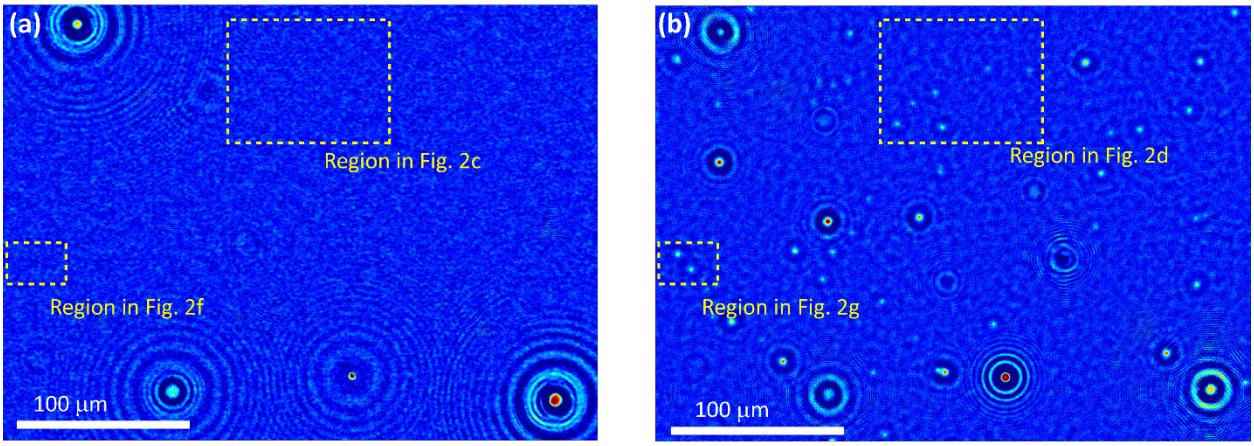

Fig. S1 Larger field of view corresponding to Fig. 2c,d,f,g showing registration among the images. The largest landmarks are visible in both the 'before' image (a) and the 'after' image (b), and can therefore be used to register the two images and make sure that we are looking at exactly the same regions of interest.

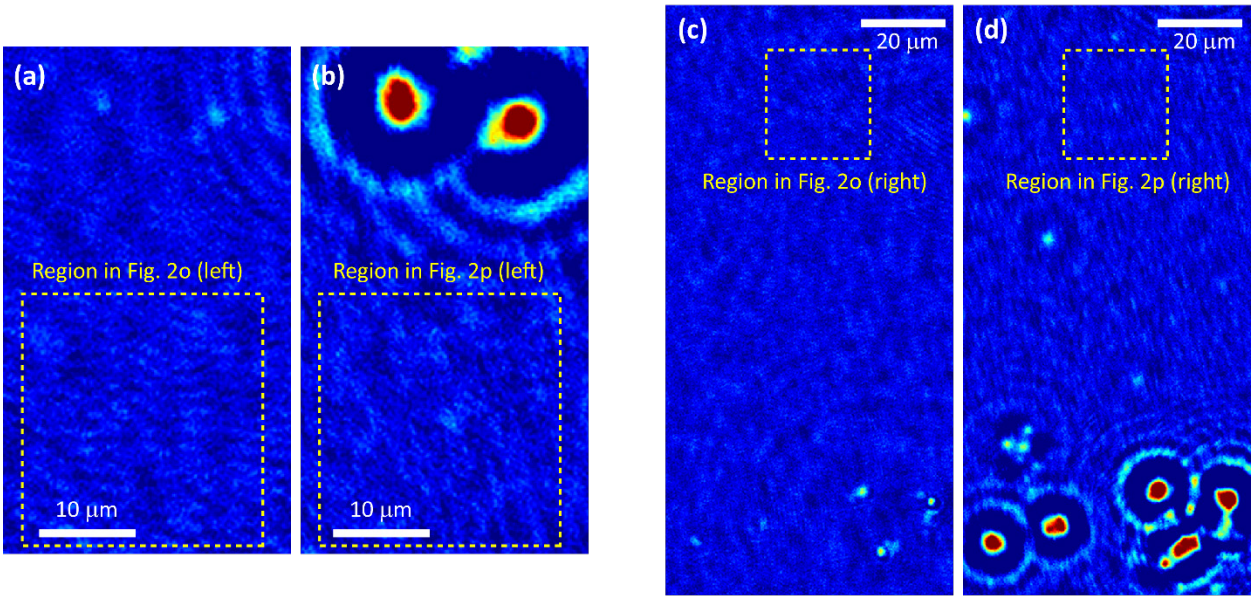

Fig. S2 Larger fields of view corresponding to Fig. 2o,p showing registration between the two images. The largest landmarks are visible in both the 'before' images (a and c) and the 'after' images (b and d), and can therefore be used to register the images and make sure that we are looking at exactly the same regions of interest.

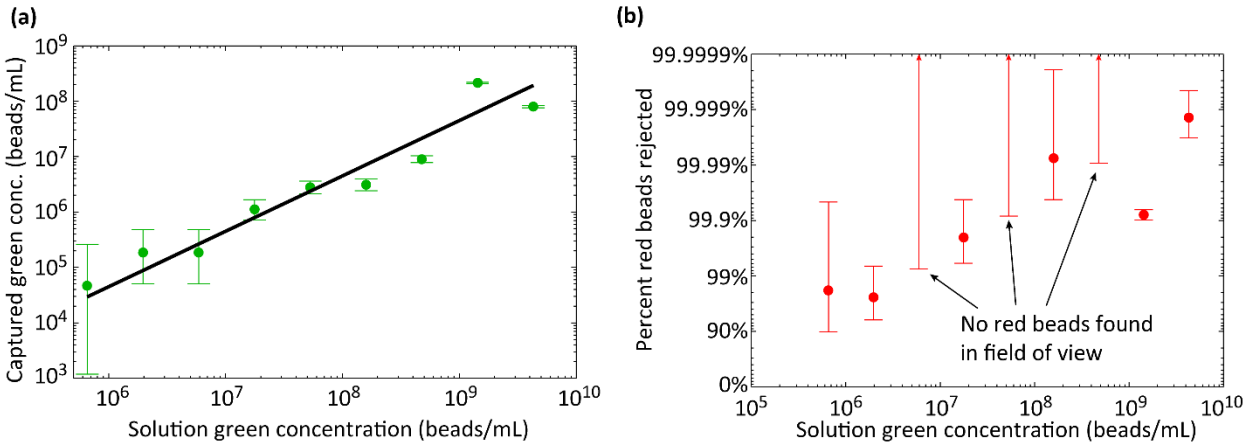

Fig. S3 Sensitivity and specificity of streptavidin-coated bead capture. These curves are measured using fluorescent microscopy, before condensation of nanolenses, and should be considered a supplement to Fig. 3 of the main text, where the specific capture of streptavidin-coated green beads is shown.

(a) Capture sensitivity. The solution green concentration (C_{sol}) is measured by letting a 0.5 µL drop of the second-most dilute solution evaporate on a cover glass, and subsequently counting each green bead in this droplet (983 beads). This concentration is then extrapolated to the 8 other dilutions using the known dilution ratio between each solution (3X). The captured green concentration (C_{capt}) is measured for each sample by counting the total number of green beads (n_g) in two non-overlapping 20X objective fields of view and computing the ratio,

$$C_{capt} = \frac{n_g\, A_{tot}}{A_{obs}\, V_{drop}},$$

where A_{tot} is the entire droplet area, A_{obs} is the total observed area, and V_{drop} is the droplet volume. For the low dilutions, only a handful of green beads may be detected, and thus Poisson statistics become significant. The error bars represent a $(1-\alpha) = 95\%$ confidence interval calculated using the formula,[1]

$$\frac{1}{2}\chi^2\left(\frac{\alpha}{2}; 2k\right)\frac{A_{tot}}{A_{obs}\, V_{drop}} \leq C_{capt} \leq \frac{1}{2}\chi^2\left(1-\frac{\alpha}{2}; 2k+2\right)\frac{A_{tot}}{A_{obs}\, V_{drop}},$$

where k is the number of green beads counted, and $\chi^2(P;\nu)$ is the inverse cumulative distribution function of the chi-squared distribution for probability P and degrees of freedom ν. The solid black line shows the best fit under the assumption $C_{capt} = \beta\, C_{sol}$, where β is a constant that describes the capture efficiency, or sensitivity, of the procedure. Here we find $\beta = 0.045$.

(b) Capture specificity. This plot shows the degree to which non-specific binding of plain red beads is mitigated for each sample, compared to the total number of red beads in each solution. These values and error bars are calculated similarly to those in panel (a), but based on the number of red beads instead of the number of green beads. In all cases, more than 90% of the red beads are washed away without being bound to the surface.

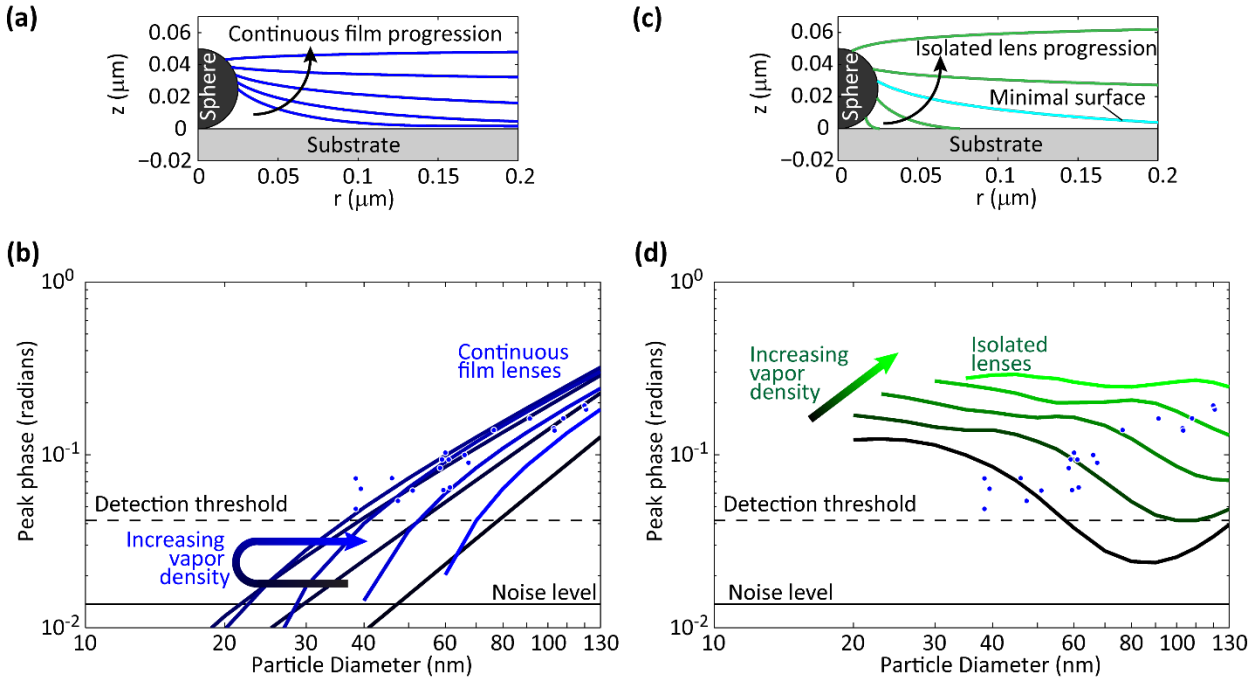

Fig. S4 Comparison between film-wise and drop-wise condensation models. **(a)** Evolving lens shapes based on film-wise condensation. This figure shows the same content as main text Fig. 1, reproduced here to facilitate comparison between the film-wise and drop-wise lens shapes. The five curves shown here were calculated using an effective vapor density of 3.61×10^{15} molecules/m^3, at times of 29 s, 49 s, 119 s, 412 s, and 1000 s. **(b)** Simulation predictions of the effect on the recovered phase signal of film-wise condensed nanolenses (black-blue curves) around spheroids after two minutes (120 s) of condensation time. Experimental measurements are shown as blue dots (reproduced from main text Fig. 4). As the effective vapor density increases from 1.29×10^{15} to 21.4×10^{15} molecules/m^3, the film-wise model predicts initially increasing phase signal, followed by a decaying phase signal (see also main text Fig. 5). Simulation predictions near the optimal vapor density fit the experimental data relatively well. **(c)** Growth of isolated lenses resulting from drop-wise condensation, assuming a substrate contact angle of 2.5°. See supplemental methods section for how these shapes are calculated. One of these shapes (shown in cyan) corresponds to a minimal surface catenoid shape, which is a type of nanolens that has previously been self-assembled around nanoparticles.[2] The effective vapor density used in these calculations was 21.4×10^{15} molecules/m^3, and the times were 33 s, 67 s, 110 s, 195 s, and 434 s. **(d)** Similar to (b) but for drop-wise condensed nanolenses. This model shows increasing phase signal over the range of vapor densities, 21.4×10^{15} to 46.8×10^{15} molecules/m^3, however none of these curves provide a good fit to the experimental data. Therefore, we conclude on the validity of our film-wise condensation model rather than drop-wise condensation.

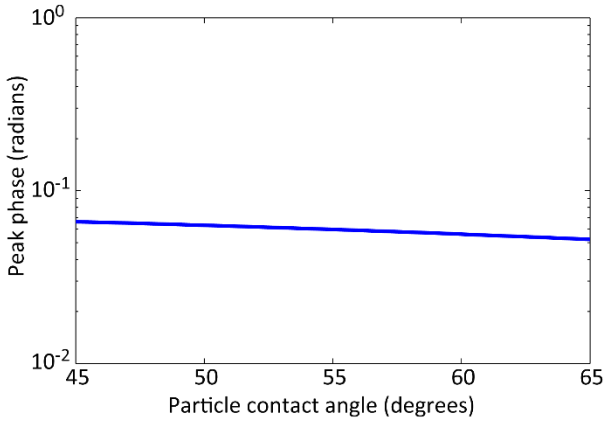

Fig. S5 Simulated signal from 50 nm spheres as a function of particle contact angle. The phase signal is somewhat insensitive to particle contact angle, and only varies $\sim \pm 10\%$ across this range of contact angles.

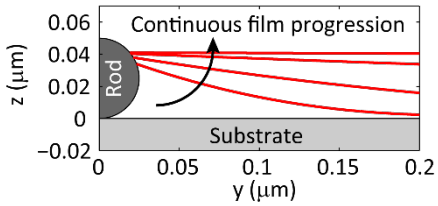

Fig. S6 Continuous-film nanolenses deposited around cylindrical rods. The time and vapor density values are the same as in the main text Fig. 1a and Supplementary Fig. S4a: vapor density of 3.61×10^{15} molecules/m^3, and times of 29 s, 49 s, 119 s, and 412 s. At a time of 1000 s, rods would be completely buried under a continuous film, even though spheres of the same diameter would 'not' (uppermost solution in Supplementary Fig. S4a). Rod-shaped particles tend to generate larger lenses than spheroidal particles for the same level of condensation.

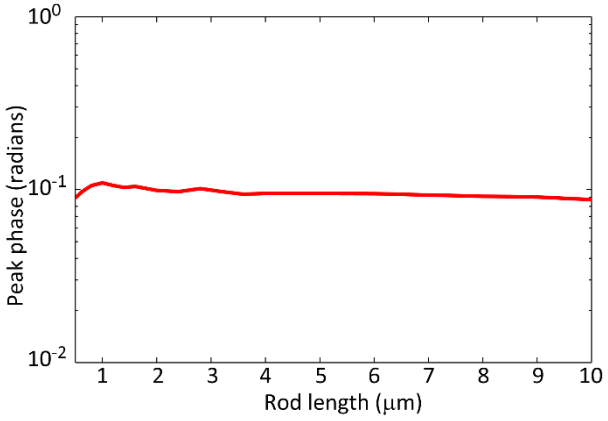

Fig. S7 Recovered signal for 30-nm-diameter rod-shaped particles as a function of particle length. Rods between 500 nm and 10 μm only show a small variation ($< \pm 15\%$) in recovered peak phase signal. All other simulation results presented in the main text and supplementary information assume a rod length of 5 μm.

Supporting Methods: Modeling the shape of isolated nanolenses formed through drop-wise condensation. Here we highlight the differences in modeling between isolated nanolenses around spherical particles (e.g. Supplementary Fig. S4a) and continuous-film nanolenses (e.g. Supplementary Fig. S4b). It is recommended to read the main methods section on lens shape modeling before this section.

First, we construct a library of possible isolated nanolens shapes by solving the Young-Laplace equation,

$$\Delta p = \rho_{PEG}\, g\, h(r) - 2\,\gamma\, K_m(r, h(r)),$$

with the two boundary conditions of the contact angle at the particle and the contact angle at the substrate. This form of the Young-Laplace equation does not include the disjoining pressure used in the form for continuous films because we are looking for solutions where the height of the lens (h) goes to zero at the edge of the lens, and the disjoining pressure $\Pi(h) \to -\infty$ as $h \to 0$, which would lead to diverging solutions.

We use the same approach as presented in the main methods section to solve the Young-Laplace ODE, namely numerically solving initial value problems for different contact heights on the sphere until a solution is found that satisfies the second boundary condition, here the contact angle at the substrate (in the main Methods section, the second boundary condition is the film thickness at infinity). In this manner, we create a library of solutions to the Young-Laplace equation for many different values of Δp, a few of which are shown in Supplementary Fig. S4b. Each solution in this library corresponds to a lens with a different volume (V) and different liquid-vapor surface area (A_{lv}). Based on this library, we can establish the relationship between surface area and volume, writing $A_{lv} = A_{lv}(V)$.

We then make the assumption that during condensation, the relative nucleation barriers are such that condensation occurs in the crack between the particle and substrate much faster than condensation anywhere else (i.e. the bare substrate, other parts of the nanoparticle, and the homogeneous vapor phase), so that these other forms of condensation may be neglected. The rate of condensation may then be expressed as,

$$\frac{dV}{dt} = J\, V_1\, A_{lv}(V),$$

where J is the molecular flux given in the main methods section, and V_1 is the volume of a single PEG molecule. The initial condition for this ODE depends on the time required to form a critical nucleus at the crack between the particle and substrate. Here we assume this time is very fast compared to the later growth dynamics. The ODE can then be solved to give the volume of the nanolens as a function of time, which can be used to identify the corresponding nanolens shape. These shapes are used to optically model the nanolens system in the same way as discussed in the main methods section, with the resulting curves plotted in shades of green in Supplementary Fig. S4c.

Supporting References

(1) Ross, S. M. *Introduction to Probability and Statistics for Engineers and Scientists*; Academic Press: San Diego, CA, 2000.

(2) Mudanyali, O.; McLeod, E.; Luo, W.; Greenbaum, A.; Coskun, A. F.; Hennequin, Y.; Allier, C. P.; Ozcan, A. Wide-Field Optical Detection of Nanoparticles Using on-Chip Microscopy and Self-Assembled Nanolenses. *Nat. Photonics* **2013**, *7*, 247–254.